

Flow arrest intra-arterial delivery of small TAT-decorated and neutral micelles to gliomas

Juliane Nguyen¹ · Shaolie S. Hossain^{2,3} · Johann R. N. Cooke⁴ · Jason A. Ellis⁵ · Michael B. Deci¹ · Charles W. Emala⁴ · Jeffrey N. Bruce⁵ · Irving J. Bigio^{6,7} · Robert M. Straubinger^{1,8} · Shailendra Joshi^{4,9}

Received: 30 October 2016 / Accepted: 9 April 2017
© Springer Science+Business Media New York 2017

Abstract The cell-penetrating trans-activator of transcription (TAT) is a cationic peptide derived from human immunodeficiency virus-1. It has been used to facilitate macromolecule delivery to various cell types. This cationic peptide is capable of crossing the blood–brain barrier and therefore might be useful for enhancing the delivery of drugs that target brain tumors. Here we test the efficiency with which relatively small (20 nm) micelles can be delivered by an intra-arterial route specifically to gliomas. Utilizing the well-established method of flow-arrest intra-arterial injection we compared the degree of brain tumor deposition of cationic TAT-decorated micelles versus

neutral micelles. Our in vivo and post-mortem analyses confirm glioma-specific deposition of both TAT-decorated and neutral micelles. Increased tumor deposition conferred by the positive charge on the TAT-decorated micelles was modest. Computational modeling suggested a decreased relevance of particle charge at the small sizes tested but not for larger particles. We conclude that continued optimization of micelles may represent a viable strategy for targeting brain tumors after intra-arterial injection. Particle size and charge are important to consider during the directed development of nanoparticles for intra-arterial delivery to brain tumors.

✉ Shailendra Joshi
sj121@cumc.columbia.edu

¹ Department of Pharmaceutical Sciences, University at Buffalo, State University of New York, Buffalo, NY, USA

² Institute for Computational Engineering and Sciences, University of Texas at Austin, Austin, TX, USA

³ Department of Molecular Cardiology, Texas Heart Institute, Houston, TX, USA

⁴ Department of Anesthesiology, Columbia University Medical Center, New York, NY, USA

⁵ Department of Neurological Surgery, Columbia University Medical Center, New York, NY, USA

⁶ Department of Electrical Engineering, Boston University, Boston, MA, USA

⁷ Department of Biomedical Engineering, Boston University, Boston, MA, USA

⁸ Department of Pharmacology & Therapeutics, Roswell Park Cancer Institute, Buffalo, NY, USA

⁹ Department of Anesthesiology, College of Physicians and Surgeons, Columbia University, 630 West 168th Street, P&S Box 46, New York, NY 10032, USA

Keywords Adjuvant therapy · Blood–brain barrier · Brain tumor · Chemotherapy · Drug delivery · Glioblastoma

Introduction

Intra-arterial (IA) drugs have been used to treat gliomas over the last five decades but the technology has remained largely investigational [1, 2]. In flow arrest intra-arterial (FA-IA) delivery, small boluses of drugs are injected into an artery during transient flow stoppage either using an occluding balloon catheter [3] or adenosine-induced cardiac pause [4, 5]. This approach overcomes several issues associated with conventional IA chemotherapy to the brain in which drugs are either diluted by the blood flow during infusion or are not absorbed due to rapid transit through the cerebral circulation [6–8]. In contrast, when drugs are injected during transient flow arrest, they can momentarily displace blood from the cerebral circulation [6]. This increases the regional arterial blood drug concentration and drug transit time. Blood cell and protein binding as well as

hemodynamic shear stress on the delivered drug molecules greatly decrease.

We have previously reported robust uptake of relatively large 80–200 nm cationic liposomes when delivered by the FA-IA method to the brain and more specifically to gliomas [9]. Increased macromolecule interaction with the cerebral vascular endothelium appeared to favor absorption of these larger cationic liposomes. However, brain tumor uptake was not always consistent possibly resulting from the large particle sizes utilized. Therefore in this study, we have endeavored to investigate the feasibility of brain tumor delivery using optimized molecules on a smaller size scale. Here we compare tumor uptake of 20 nm micellar particles decorated with the cationic human immunodeficiency virus-1 trans-activator of transcription (TAT) versus neutral micelles in a rat glioma model. Additionally, we performed simulations of a broad range of particle sizes to further inform our results.

Materials and methods

Micelle preparation

TAT-modified cysteine (GRKKRRQRRRPQC) was added to PEG-DSPE(2000) Maleimide dispersed in phosphate buffered saline (PBS) at pH 7.4 and incubated at room temperature for 4 h under constant shaking. Unreacted TAT peptide was removed using a molecular weight cut-off column (Pierce Concentrator). Micellar carriers were prepared as described previously [10]. Briefly, DSPE-mPEG(2000) (Avanti Polar Lipids, Alabaster, AL) or a 20/80 mixture of DSPE-PEG(2000)-TAT/PEG-DSPE(2000)-amine were mixed with 1,1'-dioctadecyl-3,3,3',3'-tetramethylindodicarbocyanine, 4-chlorobenzene-sulfonate salt at a molar ratio of 98/2. The PEGylated lipid mixture was then dried to a thin PEG-lipid film using a rotary evaporator followed by rehydration of the lipid film in phosphate buffered saline (PBS) and sonication for 10 min at room temperature

until fully dispersed. The particle sizes of the TAT-decorated DSPE-PEG(2000)-amine and methoxy-PEG-DSPE (mPEG-DSPE) micelles were measured by dynamic light scattering (DLS) using the Nanobrook Omni (Brookhaven Instruments Corp., Holtville, NY). To determine the effect of pH on zeta potential, the micelles were dispersed in PBS at pH 7.4 and in 20 mM of 2-(*N*-morpholino) ethanesulfonic acid (MES) buffer at pH 6.5, 6.0, and 5.5 [11]. Three measurements were taken per sample and represented as mean \pm standard deviation.

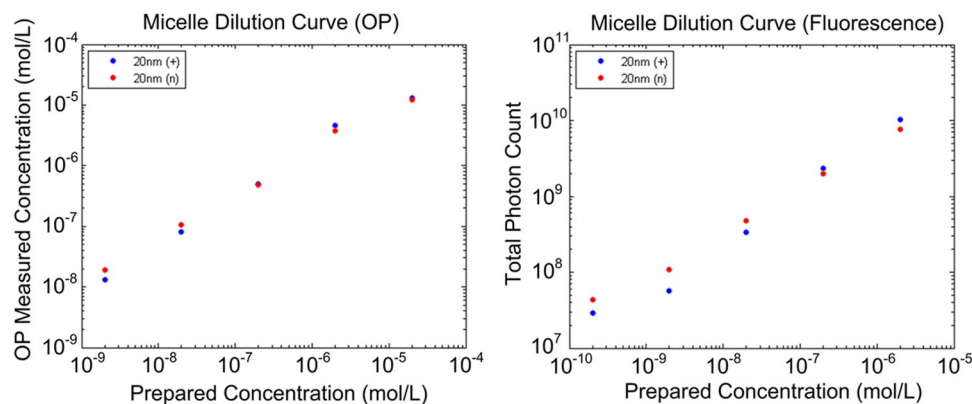
In vitro spectroscopy

DiD-labeled micelles were dissolved in 10% intralipid and concentrations were compared to concentrations measured by diffuse reflectance spectroscopy (DRS) and semi-quantitative fluorescence imaging [12–15]. A custom built device (Optimum Technologies Inc., Boston, MA) employing a xenon light source to generate white light (450–850 nm) delivered to the target site via a fiber optic cable was used for DRS. In this setup, the backscattered light is relayed to a spectroscope via another cable and is subjected to spectral analysis to determine tracer and drug concentrations. For semi-quantitative fluorescence imaging, a 635 ± 5 nm LED light excitation was imaged through a 680 ± 5 nm band-pass filter using an electron multiplying charge-coupled device (EMCCD, Evolve 512, Photometrics Inc., Huntington Beach, CA). The camera corrects for background noise and can quantify the photon yield. The dissolved concentrations were compared to concentrations measured by DRS and semi-quantitative fluorescence imaging, which were closely correlated (Fig. 1).

In vivo studies

Institutional Review Board and Animal Care and Use Committee approvals were obtained for all studies. Rodent gliosarcoma cells (9L) were cultured to confluence in T25 flasks in Dulbecco's modified Eagle's medium (DMEM)

Fig. 1 Spectroscopy and fluorescence concentration measurements. Measurement of concentrations by diffuse reflectance spectroscopy (*left*) and total photon count (*right*) in a tissue phantom are shown. A linear correlation is seen between measured and known increasing concentrations of 20 nm TAT-decorated and neutral micelles using both techniques



with 10% fetal bovine serum and penicillin/streptomycin and kept humidified at 37 °C with 5% CO₂. The 9L tumor model has similar blood–brain barrier permeability properties to human gliomas making it a reasonable model for these IA delivery studies [16–18]. On the day of implantation, cells were trypsinized, washed, and re-suspended to 4×10^5 cells (85–95% viability) in 5 μ l of basal DMEM. Stereotactic implantation was performed using a 33-G Hamilton needle 2 mm posterior, 3 mm lateral, and 3.5 mm deep to the bregma over the right hemisphere.

Power analysis based on a conservative 50% effect yielded a necessary sample size of 6 animals to demonstrate a difference. Experiments were conducted on two groups of Fisher 344 rats: Group 1 rats ($n = 14$) had tumors growing for a mean of 15 ± 1 days prior to injection of a high dose of 0.6 ml stock micelles, and Group 2 rats ($n = 8$) had tumors growing for a mean of 13 ± 1 days prior to injection a lower dose of 0.2 ml stock micelles. All animals were confirmed to be asymptomatic from their brain tumor prior to IA injection of micelles.

Surgical procedures were carried out under general ketamine and isoflurane anesthesia. A tail vein line, tracheostomy, and right common carotid catheter were placed, followed by ligation of all branches of the external carotid artery. The DRS probe was placed over the right parietal region in Group 1 and close to the site of tumor implantation in Group 2. To monitor cerebral blood flow (CBF), a laser Doppler probe was placed just in front of the coronal suture over the right frontal region. In addition, the inspired and exhaled gas composition, skin blood flow, electrocardiogram, pulse oxygen saturation and volume, and rectal temperature were monitored. All physiological data were recorded in real-time by Mac-Lab software (AD Instruments, Boston, MA). DRS measurements recorded tissue tracer concentrations with each micelle injection over a period of approximately 30 min. The first twelve baseline measurements were taken over 1 min, then 300 measurements were taken 500 ms apart, and finally 300 measurements were 5000 ms apart.

IA drugs were injected using a pneumatic 1 ml syringe with a Parker III injector controlled by an Agilent II Signal generator (Applied Signal Inc., Sunnyvale, CA). Hypotension was induced with a bolus intravenous injection of adenosine (2–3 mg), esmolol (2–3 mg), and cold saline (4 °C, 1.5 ml). Pulsed intracarotid injections (60–70 μ l) were delivered every 2 s such that micelles were injected within 30 s of peak hypotension (Fig. 2).

Micelle characterization

Micelle size was determined by dynamic light scattering (DLS). TAT-decorated micelles displayed a hydrodynamic diameter of 21.8 ± 6.4 nm and the micelles composed of

PEG-lipid-containing non-ionizable methoxy groups displayed a hydrodynamic diameter of 21.46 ± 2.98 nm. Zeta potential measurements were used to characterize the pH-dependent surface charge of the neutral micelles and TAT-decorated micelles (Table 1).

Simulation studies

Considering the nanoparticles as passive scalars, the mass transport of nanoparticles in blood flow is governed by the linear advection-diffusion-reaction equation [19]. As detailed in previous work [20], the adhesion of blood-borne spherical nanoparticles to the vessel wall is directly influenced by the local wall shear rate S , the particle diameter d_p , and the probability of adhesion P_a . The probability of adhesion P_a is a measure of the strength of adhesion and can be thought of as the propensity of nanoparticles, liposomes, or micelles to stably adhere to the vessel wall overcoming the hemodynamic forces that tend to displace them. P_a is modeled as a function of nanoparticle design parameters such as size, shape and surface characteristics including charge density and the avidity between the cationic nanoparticle and anionic blood vessel wall; as well as certain physiological parameters such as the local wall shear rate and the disease state of the vessel wall. The particle adhesion model was validated against a range of spherical particle sizes and wall shear rate. Readers are referred to previously published work for further details [20, 21].

Particle adhesion is known to be strongly modulated by the deposition parameter Π defined as $\Pi = P_a S d_p / 2$ and consequently, the probability of adhesion [20]. A MATLAB (8.4.0.150421 Release 2014b, The MathWorks Inc., Natick, Massachusetts) code was used to estimate the particle adsorption rate (deposition parameter) and probability of adhesion for a range of relevant particle sizes and wall shear rate mimicking the experimental conditions in order to enhance our understanding of the underlying physics and gain further insight into experimental observations.

Data analysis

Stat View 5.2 (SAS Institute, Cary NC) was used to perform ANOVA and factorial ANOVA where appropriate. Bonferroni correction was used when multiple comparisons were made. Statistical significance was set at $p \leq 0.05$.

Results

In vitro phantom tissue experiments

The dissolved concentrations were compared to concentrations measured by diffuse reflectance spectroscopy (DRS)

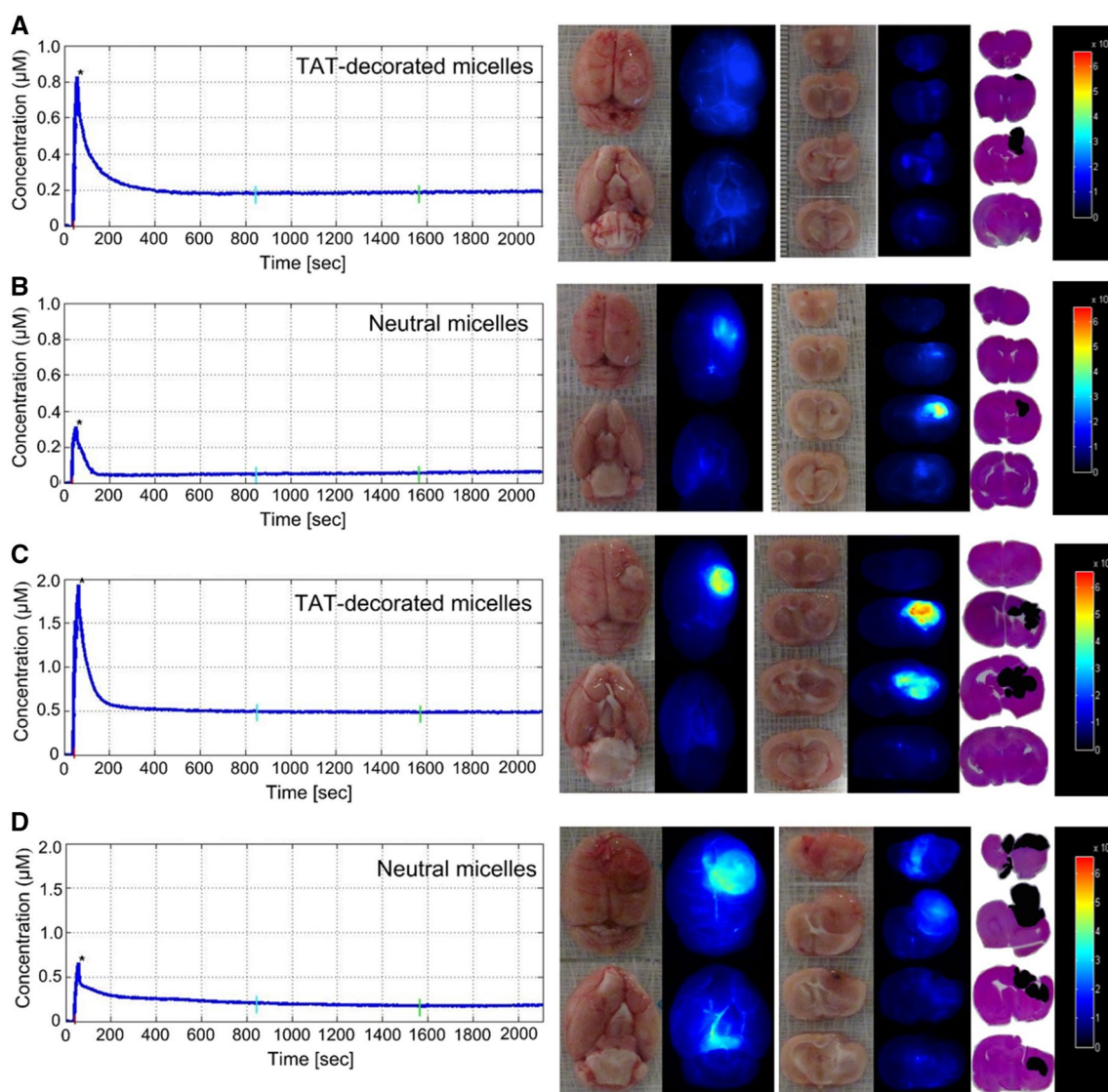


Fig. 2 Uptake of TAT-decorated and neutral micelles by gliomas. Data from both low dose (**a, b**) and high dose (**c, d**) injections are shown. The concentration–time curves (*left panel*) indicate tumor surface kinetics with micelle clearance recorded for over 30 min

Table 1 pH-dependent zeta potential of TAT-decorated micelles and neutral micelles

pH	TAT micelles (mV)	Neutral micelles (mV)
5.5	16.8 ± 7.7	-5.9 ± 1.7
6.0	13.0 ± 4.4	-2.6 ± 2.5
6.5	8.4 ± 3.0	-4.8 ± 1.3
7.4	7.1 ± 1.4	-3.6 ± 1.2

and semi-quantitative fluorescence imaging. Both diffuse reflectance spectroscopy and fluorescence measurements correlated well with the dissolved micelle concentrations

(1800 s) after injection (0–200 s). Corresponding gross, fluorescence, and histology images are shown (*right panel*). The localized high intensity fluorescence signal indicates glioma-specific uptake of the micelles

(Fig. 1). Therefore the optical pharmacokinetic strategies utilized for in vivo and post-mortem experiments provide an accurate representation of directly measured tissue concentrations.

In vivo experiments

In vivo experiments were conducted on 22 rats split into high injection dose (0.6 ml micelles) and low injection dose (0.2 ml micelles) groups as previously described. Technical issues with carotid cannulation necessitated one animal from the high-dose group be excluded from further analysis. As expected, the high-dose injection animals

had somewhat larger tumors than the low-dose injection animals since tumors were allowed to grow for longer in the high dose group. No clinical difference was observed in animals injected with neutral versus cationic TAT-decorated micelles. The hemodynamic data, heart rate, skin blood flow, and cerebral blood flow showed similar changes between TAT-decorated and neutral micelles. There was an expected decrease in hemodynamic parameters during flow arrest that subsequently recovered (Table 2).

Diffuse reflectance spectroscopy

Tumor deposition of both TAT-decorated and neutral micelles was noted after intra-arterial injection. Surface measurements of tracer concentrations of the two micelle formulations showed higher values for TAT-decorated micelles. This was evident in both the high and low dose animal groups. However, the observed trend toward increased uptake of TAT-decorated micelles was not statistically significant. Thus, the quantitated parameters including peak concentration, end concentration, and area under the concentration–time curve were not statistically different between the TAT-decorated micelles and the neutral ones (Table 2).

Postmortem image analysis

Postmortem image analysis showed effective, consistent, and targeted uptake of both neutral and TAT-decorated micelles by the gliomas (Fig. 2). No obvious differences were noted in the deposition pattern between TAT-decorated micelles and neutral micelles. There was also deposition of both micelle types along the blood vessels, particularly around the Circle of Willis. Expected increased delivery concentration in the high injection dose group was seen.

Simulations

The simulations performed show how nanoparticles size and surface charge are predicted to affect regional brain deposition. A wide range of nanoparticle sizes from 10 to 500 nm for a variety of relevant hemodynamic condition in terms of wall shear rate were tested. At 80 nm or larger, there is increased deposition at low shear stresses which can be clinically achieved with flow arrest. However as the wall shear stress increases the deposition of larger particles also decreases dramatically. Cationic charge increases both the deposition rate and probability of adhesion under FA-IA for these larger particles. However, the significance

Table 2 Tumor size, tissue concentrations and hemodynamics

	High dose		Low dose	
	Neutral (n=6)	TAT (n=7)	Neutral (n=4)	TAT (n=4)
<i>Tumor sizes</i>				
Tumor volume gross image	175 ± 161 mm ³	145 ± 90 mm ³	34 ± 35 mm ³	59 ± 33 mm ³
Tumor volume histology	102 ± 95 mm ³	93 ± 59 mm ³	41 ± 27 mm ³	42 ± 27 mm ³
<i>Diffuse Reflectance spectroscopy</i>				
Peak Conc.(mMol)	1.91 ± 0.87	2.44 ± 1.12	0.44 ± 0.11	0.59 ± 0.23
End Conc (mMol)	0.31 ± 0.20	0.32 ± 0.19	0.05 ± 0.02	0.15 ± 0.13
AUC (mMol.s)	293 ± 212	318 ± 175	37 ± 10	115 ± 60
<i>Heart rate (BPM)</i>				
Base	291 ± 34	260 ± 43	222 ± 22	238 ± 23
Injection	135 ± 85	110 ± 45	59 ± 12	77 ± 16
5 min	283 ± 27	266 ± 37	228 ± 22	233 ± 26
End	287 ± 18	277 ± 23	233 ± 16	254 ± 8
<i>LD brain (%Δ baseline)</i>				
Base	100 ± 0	100 ± 0	100 ± 0	100 ± 0
Injection	17 ± 3	13 ± 5	25 ± 27	14 ± 27
5 min	95 ± 25	125 ± 41	115 ± 22	115 ± 22
End	73 ± 33	42 ± 30	85 ± 26	85 ± 26
<i>Laser Doppler skin (%Δ baseline)</i>				
Base	100 ± 0	100 ± 0	100 ± 0	100 ± 0
Injection	14 ± 6	11 ± 3	13 ± 7	14 ± 7
5 min	108 ± 30	98 ± 38	127 ± 30	129 ± 45
End	106 ± 33	49 ± 38	120 ± 11	87 ± 33

§ Significant difference from baseline, # Significant difference between TAT and neutral micelles

of charge lessened with small nanoparticle sizes. Indeed the computational simulations show that particle charge effects an almost negligible consequence for the deposition of 20 nm nanoparticles such as the micelles we injected (Fig. 3).

Discussion

Contrary to our previous findings that cationic surface charge plays a major role in regional liposome (large nanoparticle) deposition [7, 22, 23], here we detected no benefits from the application of a cationic charge to smaller 20 nm micelles. Indeed, at this particle size both neutral and cationic micellar preparations penetrated tumors effectively after intra-arterial injection. We also noted deposition along blood vessels, particularly the Circle of Willis, with both preparations. Ante-mortem measurements of tissue concentrations by DRS showed no significant difference between the two particles delivered.

Flow arrest drug delivery has been long used to treat cancers in organs such as the liver, breast, and eye. However, it is a relatively new method of drug delivery for the treatment of brain tumors. To date, only a single clinical case utilizing this method in a brain tumor patient has been reported [3]. In other scenarios this technique has gained some traction including transient cardiac pause with intravenous adenosine to treat high flow arteriovenous malformations and local flow arrest with temporary clipping during aneurysm, carotid, cerebral bypass and other neurovascular surgeries [4, 5, 24]. Thus there exists an ample safety record for the clinical use of transient flow arrest to the brain in humans. The routine utilization of transient flow arrest during neurovascular surgery makes a compelling case that momentary flow interruptions are both feasible and safe and could be used to improve drug delivery to the brain.

The impact of flow arrest drug delivery on the pharmacokinetic paradigm of IA drug delivery is often overlooked. Brain tissue has a very high basal blood flow, which greatly

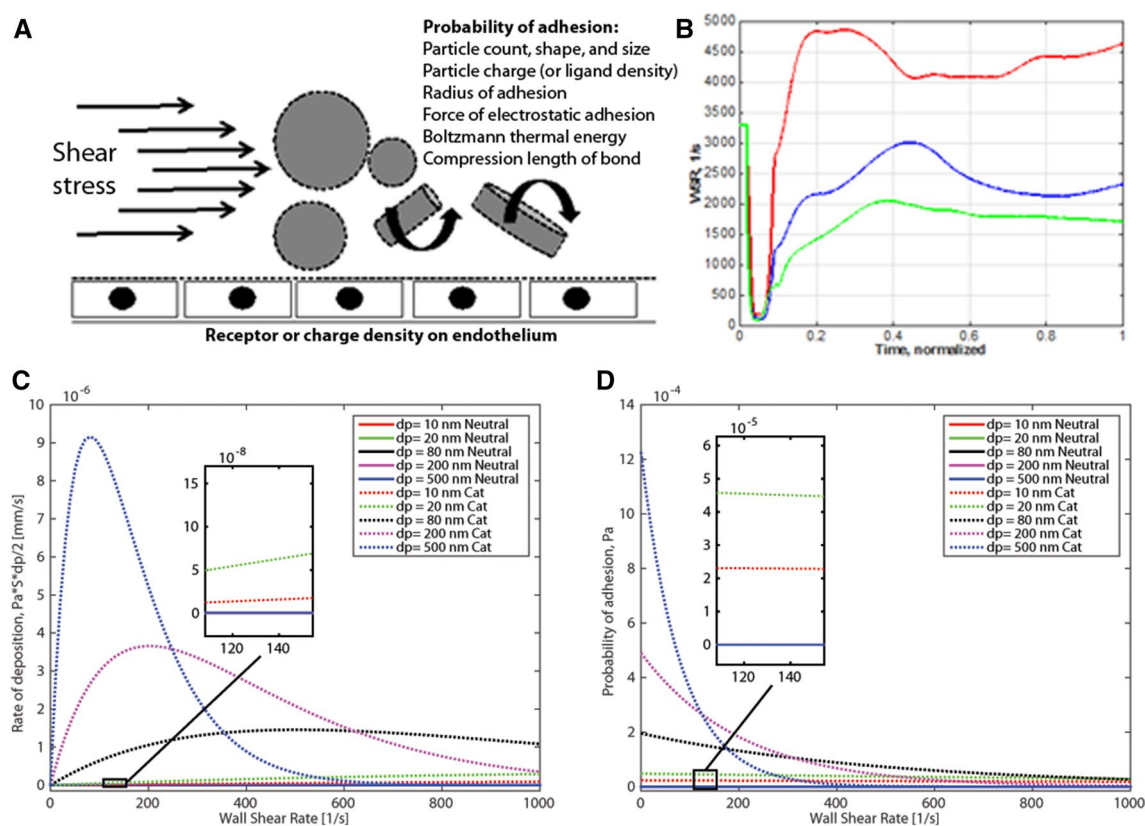


Fig. 3 Computational modeling IA nanoparticle delivery to the brain. Nanoparticle interaction and consequently the probability of particle adhesion to the endothelial surface are determined by a range of physical characteristics as noted in the schematic of a cerebral blood vessel (a). Using a range of experimental hemodynamic data during flow-arrest drug delivery, we calculated wall shear stress (b). Rates of particle uptake (c) and the probability of adhesion (d) to the

vascular endothelium as a function of wall shear rate for cationic and neutral particles in sizes ranging from 10 to 500 nm are shown. These simulations show that decreased wall shear stress (<500 1/s) such as during FA-IA drug delivery will increase the probability of adhesion of larger particles. This effect is seen to be minimal for small particle sizes approximating 20 nm as noted during in vivo delivery analysis

decreases the benefits of IA injections. IA bolus injections during flow arrest increase arterial blood concentration, increase drug transit time, prevent or minimize non-targeted binding with blood proteins and cells, and decrease the shear stress on particles to improve targeted uptake. Thus, flow arrest can greatly improve targeted drug delivery. We recently modeled flow arrest-IA drug delivery by elaborating the Dedrick model and simulation showed that the benefits of FA-IA drug delivery were significant when there is rapid uptake and retention by tumor tissue [25–27].

Computer simulation reported here shows how decreasing shear stress facilitates the delivery of large cationic particles (>80 nm). As the local wall shear stress increases, these large particles experience greater drag force compared to smaller particles. At the same time, the larger the particle size, the greater the surface area available for adhesive interaction with the vessel wall. As a result, the attractive forces between the cationic particle and anionic vessel wall can better overcome the relatively low hydrodynamic stresses prevailing during FA-IA delivery, leading to firm particle adhesion. In this scenario, the attractive forces between the positively charged particles and the negatively charged endothelium are critical to promoting adhesion and absorption. This is relevant for particles between 80 and 500 nm in size. With decreasing particle sizes (≤ 20 nm), the area of interaction decreases, reducing the adhesive forces between the particle and endothelium. As a result, the probability of adhesion, and consequently the rate of deposition, is lower for smaller particles during FA-IA delivery. According to the simulations, the effect of surface charge on particle adhesion would be largest for size ranges between 80 and 500 nm. For the small 20 nm particles utilized in this set of experiments, the effects due to surface charge seemed to be minimal.

Prior to conducting these insightful computational studies, we hypothesized that decorating micelles with TAT would greatly improve drug delivery due, in part, to its positive charge and result in enhanced regional drug deposition. We were initially surprised to find that this was indeed not the case with improvements in regional delivery of TAT-decorated micelles being much less robust than was previously noted in experiments utilizing larger liposomes. A posteriori, our simulation studies support the experimental data. Perhaps a better strategy for improving tumor delivery of micelles is to trap them in the acidic pH of the tumor through ionization after uptake as we have previously shown [27].

The question of whether tumor uptake efficiency is influenced by tumor size was not directly addressed in this report. Although the Group 1 and Group 2 experiments had different gross tumor volumes, all statistical comparisons were made within each independent group experiment. This will be an important avenue for

investigation in future experiments since we believe that: (1) large tumors with a complex vascular supply may show uneven, heterogeneous uptake, (2) large tumors may have higher interstitial hydrostatic pressures that could affect drug uptake and clearance and (3) large tumors might have more physiological variability including regions of ischemia, hemorrhage, and necrosis with microcirculatory failure all of which can affect uptake efficiency [28, 29].

Several different mechanisms have been proposed to explain TAT facilitated macromolecule uptake into cells [30]. This includes adsorptive endocytosis and direct fusion with the cellular membrane. The exact mechanism of TAT-decorated micelle uptake, however, remains unclear. Our ongoing studies have shown rapid uptake of TAT-FITC by cancer cells and after FA-IA delivery [31]. At the molecular level, TAT-conjugated FITC is robustly taken up by brain tumors when delivered by FA-IA injection but when TAT is conjugated to larger proteins such as GFP, TAT-GFP proteins are taken up less than the equimolar amounts of TAT and GFP when co-administered in cell cultures [32]. It seems that both the size and rigidity of the molecules might play a role in TAT-enhanced drug delivery. Micelle formulations might be taken up by brain tumors utilizing other mechanisms, such as by increased lipid solubility. Because of their surfactant-like behavior, micelles are capable of undergoing lipid transfer and exchange with cellular membranes. As a result, the membrane dye DID—which is incorporated into the micelles—may have been transferred to the cellular membrane after FA-IA delivery. This alternate mechanism of uptake is equally applicable to TAT-decorated and neutral micelles and therefore could explain the lack of an observed difference in uptake between the two formulations.

We conclude that both neutral and cationic micelles may be formulated to facilitate drug delivery to gliomas by the FA-IA method. At the small particle size (20 nm) tested, cationic micelles show modest delivery superiority. Future studies are warranted in additional models and to assess the surface properties of micellar carriers to gauge their ability to affect the delivery of therapeutic cargo into glioma cells.

Funding National Cancer Institute at the National Institutes of Health RO1-CA-138643.

Compliance with ethical standards

Conflict of interest The authors declare that they have no conflict of interest.

Ethical approval All applicable international, national, and/or institutional guidelines for the care and use of animals were followed. All procedures performed were in accordance with the ethical standards of Columbia University.

References

- Ellis JA, Banu M, Hossain SS, Singh-Moon R, Lavine SD, Bruce JN, Joshi S (2015) Reassessing the role of intra-arterial drug delivery for glioblastoma multiforme treatment. *J Drug Deliv* 2015:405735. doi:[10.1155/2015/405735](https://doi.org/10.1155/2015/405735)
- Joshi S, Ellis JA, Ornstein E, Bruce JN (2015) Intraarterial drug delivery for glioblastoma multiforme: will the phoenix rise again? *J Neurooncol* 124(3):333–343. doi:[10.1007/s11060-015-1846-6](https://doi.org/10.1007/s11060-015-1846-6)
- Riina HA, Knopman J, Greenfield JP, Fralin S, Gobin YP, Tsiouris AJ, Souweidane MM, Boockvar JA (2010) Balloon-assisted superselective intra-arterial cerebral infusion of bevacizumab for malignant brainstem glioma. A technical note. *Interv Neuroradiol* 16(1):71–76
- Hashimoto T, Young WL, Aagaard BD, Joshi S, Ostapkovich ND, Pile-Spellman J (2000) Adenosine-induced ventricular asystole to induce transient profound systemic hypotension in patients undergoing endovascular therapy. Dose-response characteristics. *Anesthesiology* 93(4):998–1001
- Pile-Spellman J, Young WL, Joshi S, Duong DH, Vang MC, Hartmann A, Kahn RA, Rubin DA, Prestigiacomo CJ, Ostapkovich ND (1999) Adenosine-induced cardiac pause for endovascular embolization of cerebral arteriovenous malformations: technical case report. *Neurosurgery* 44(4):881–886 (discussion 886–887)
- Joshi S, Wang M, Etu JJ, Suckow RF, Cooper TB, Feinmark SJ, Bruce JN, Fine RL (2008) Transient cerebral hypoperfusion enhances intraarterial carmustine deposition into brain tissue. *J Neurooncol* 86(2):123–132. doi:[10.1007/s11060-007-9450-z](https://doi.org/10.1007/s11060-007-9450-z)
- Joshi S, Singh-Moon RP, Wang M, Chaudhuri DB, Holcomb M, Straubinger NL, Bruce JN, Bigio IJ, Straubinger RM (2014) Transient cerebral hypoperfusion assisted intraarterial cationic liposome delivery to brain tissue. *J Neurooncol* 118(1):73–82. doi:[10.1007/s11060-014-1421-6](https://doi.org/10.1007/s11060-014-1421-6)
- Wang M, Etu J, Joshi S (2007) Enhanced disruption of the blood brain barrier by intracarotid mannitol injection during transient cerebral hypoperfusion in rabbits. *J Neurosurg Anesthesiol* 19(4):249–256. doi:[10.1097/ANA.0b013e3181453851](https://doi.org/10.1097/ANA.0b013e3181453851)
- Joshi S, Cooke JR, Chan DK, Ellis JA, Hossain SS, Singh-Moon RP, Wang M, Bigio IJ, Bruce JN, Straubinger RM (2016) Liposome size and charge optimization for intraarterial delivery to gliomas. *Drug Deliv Transl Res* 6(3):225–233. doi:[10.1007/s13346-016-0294-y](https://doi.org/10.1007/s13346-016-0294-y)
- Nguyen J, Sievers R, Motion JP, Kivimae S, Fang Q, Lee RJ (2015) Delivery of lipid micelles into infarcted myocardium using a lipid-linked matrix metalloproteinase targeting peptide. *Mol Pharm* 12(4):1150–1157. doi:[10.1021/mp500653y](https://doi.org/10.1021/mp500653y)
- Walsh CL, Nguyen J, Szoka FC (2012) Synthesis and characterization of novel zwitterionic lipids with pH-responsive biophysical properties. *Chem Commun* 48(45):5575–5577. doi:[10.1039/c2cc31710a](https://doi.org/10.1039/c2cc31710a)
- Bigio IJ, Bown SG (2004) Spectroscopic sensing of cancer and cancer therapy: current status of translational research. *Cancer Biol Ther* 3(3):259–267
- Mourant JR, Johnson TM, Los G, Bigio IJ (1999) Non-invasive measurement of chemotherapy drug concentrations in tissue: preliminary demonstrations of in vivo measurements. *Phys Med Biol* 44(5):1397–1417
- Reif R, Wang M, Joshi S, A'Amar O, Bigio IJ (2007) Optical method for real-time monitoring of drug concentrations facilitates the development of novel methods for drug delivery to brain tissue. *J Biomed Opt* 12(3):034036
- Ergin A, Wang M, Zhang J, Bigio I, Joshi S (2012) Non-invasive in vivo optical assessment of blood brain barrier permeability and brain tissue drug deposition in rabbits. *J Biomed Opt* 17(5):057008
- Wilkins DE, Raaphorst GP, Saunders JK, Sutherland GR, Smith IC (1995) Correlation between Gd-enhanced MR imaging and histopathology in treated and untreated 9L rat brain tumors. *Magn Reson Imaging* 13(1):89–96
- Fross RD, Warnke PC, Groothuis DR (1991) Blood flow and blood-to-tissue transport in 9L gliosarcomas: the role of the brain tumor model in drug delivery research. *J Neurooncol* 11(3):185–197
- Barth RF, Kaur B (2009) Rat brain tumor models in experimental neuro-oncology: the C6, 9L, T9, RG2, F98, BT4C, RT-2 and CNS-1 gliomas. *J Neurooncol* 94(3):299–312. doi:[10.1007/s11060-009-9875-7](https://doi.org/10.1007/s11060-009-9875-7)
- Hossain SS, Hossainy SFA, Bazilevs Y, Calo VM, Hughes TJR (2012) Mathematical modeling of coupled drug and drug-encapsulated nanoparticle transport in patient-specific coronary artery walls. *Comput Mech* 49(2):213–242
- Hossain SS, Zhang Y, Liang X, Hussain F, Ferrari M, Hughes TJ, Decuzzi P (2013) In silico vascular modeling for personalized nanoparticle delivery. *Nanomedicine* 8(3):343–357. doi:[10.2217/nmm.12.124](https://doi.org/10.2217/nmm.12.124)
- Hossain SS, Hughes TJ, Decuzzi P (2014) Vascular deposition patterns for nanoparticles in an inflamed patient-specific arterial tree. *Biomech Model Mechanobiol* 13(3):585–597. doi:[10.1007/s10237-013-0520-1](https://doi.org/10.1007/s10237-013-0520-1)
- Joshi S, Singh-Moon R, Wang M, Chaudhuri DB, Ellis JA, Bruce JN, Bigio IJ, Straubinger RM (2014) Cationic surface charge enhances early regional deposition of liposomes after intracarotid injection. *J Neurooncol* 120(3):489–497. doi:[10.1007/s11060-014-1584-1](https://doi.org/10.1007/s11060-014-1584-1)
- Joshi S, Singh-Moon RP, Ellis JA, Chaudhuri DB, Wang M, Reif R, Bruce JN, Bigio IJ, Straubinger RM (2015) Cerebral hypoperfusion-assisted intra-arterial deposition of liposomes in normal and glioma-bearing rats. *Neurosurgery* 76(1):92–100. doi:[10.1227/NEU.0000000000000552](https://doi.org/10.1227/NEU.0000000000000552)
- Joshi S, Ellis JA, Emala CW (2014) Revisiting intra-arterial drug delivery for treating brain diseases or is it “dejavu, all over again”? *J Neuroanaesth Crit Care* 1(2):108–115. doi:[10.4103/2348-0548.130386](https://doi.org/10.4103/2348-0548.130386)
- Cooke JN, Hossain S, Ellis JE, Joshi S (2016) Limitations of intraarterial drug delivery without optimized formulations revealed by pharmacokinetic modeling (Abstract, accepted for the Proceedings of Society of Neuroanesthesiology and Critical Care 44th Annual Meeting, Chicago IL). *J Neurosurg Anesthesiol* 28(4):493–494
- Dedrick RL (1988) Arterial drug infusion: pharmacokinetic problems and pitfalls. *J Natl Cancer Inst* 80(2):84–89
- Cooke JN, Ellis JA, Hossain S, Nguyen J, Bruce JN, Joshi S (2016) Computational pharmacokinetic rationale for intra-arterial delivery to the brain. *Drug Deliv Transl Res* 6(5):622–629. doi:[10.1007/s13346-016-0319-6](https://doi.org/10.1007/s13346-016-0319-6)
- Kang T, Zhu Q, Jiang D, Feng X, Feng J, Jiang T, Yao J, Jing Y, Song Q, Jiang X, Gao X, Chen J (2016) Synergistic targeting tenascin C and neuropilin-1 for specific penetration of nanoparticles for anti-glioblastoma treatment. *Biomaterials* 101:60–75. doi:[10.1016/j.biomaterials.2016.05.037](https://doi.org/10.1016/j.biomaterials.2016.05.037)
- Munson JM, Bellamkonda RV, Swartz MA (2013) Interstitial flow in a 3D microenvironment increases glioma invasion by a CXCR4-dependent mechanism. *Cancer Res* 73(5):1536–1546. doi:[10.1158/0008-5472.CAN-12-2838](https://doi.org/10.1158/0008-5472.CAN-12-2838)
- Madani F, Lindberg S, Langel U, Futaki S, Graslund A (2011) Mechanisms of cellular uptake of cell-penetrating peptides. *Joural Biophys* 2011:414729. doi:[10.1155/2011/414729](https://doi.org/10.1155/2011/414729)
- Joshi S, Wang M, Singh-Moon R (2013) Feasibility of intra-arterial drug delivery to brain tissue using cell penetrating

- peptides. *J Neurosurg Anesthesiol* 25(4):465. doi:[10.1097/ANA.0b013e3182a4d5ff](https://doi.org/10.1097/ANA.0b013e3182a4d5ff)
32. Lohcharoenkal W, Manosroi A, Gotz F, Werner RG, Manosroi W, Manosroi J (2011) Potent enhancement of GFP uptake into HT-29 cells and rat skin permeation by coinubation with tat peptide. *J Pharm Sci* 100(11):4766–4773. doi:[10.1002/jps.22671](https://doi.org/10.1002/jps.22671)